Experimental Verification and Capacity Prediction of FE-OCDMA Using Superimposed FBG

Simon Ayotte, *Student Member, IEEE, Student Member, OSA*, Martin Rochette, Julien Magné, Leslie A. Rusch, *Senior Member, IEEE, Member, OSA*, and Sophie LaRochelle, *Member, IEEE, Member, OSA*

***Abstract*—This paper presents the experimental demonstration and simulation results of a frequency-encoded optical code-division multiple-access (FE-OCDMA) system using broad-band incoherent source, superimposed fiber Bragg gratings for encoding/decoding of unipolar m-sequence codes, and balanced detection. The bit-error rate is measured for up to four simultaneous users at 155 and 622 Mb/s. Exploiting the excellent match between simulation and experiment, the paper concludes with a prediction of the potential capacity of an optimized FE-CDMA system.**

***Index Terms*—Fiber Bragg gratings, frequency encoding, intensity noise, optical-code-division multiple access (OCDMA).**

I. Introduction

SEVERAL optical-code-division multiple-access (OCDMA) techniques have been proposed and demonstrated to offer flexible solutions for local area networks while allowing asynchronous access to the network. Among them, direct-sequence OCDMA and fast-frequency-hopping OCDMA seem promising, but they require high electrical bandwidth for the detection of short pulses. In frequency-encoded (FE) OCDMA systems with broad-band incoherent sources [1]–[11], the receiver bandwidth is limited to the data rate, thereby offering low cost. Moreover, it has the advantage of canceling multiple-access interference (MAI) when a balanced detection is employed.

Previous studies of FE-OCDMA had limited experimental validation [2]–[7] or purely theoretical analyses [8]–[11]. In [2], the first experimental implementation of a FE-OCDMA system using superimposed fiber Bragg gratings (FBGs) for encoding/decoding operations was presented. In this paper, the performance of FE-OCDMA is demonstrated both experimentally and theoretically. Bit-error-rate (BER) measurements at 155 and 622 Mb/s are presented, showing that MAI is properly eliminated and that the performance is limited by intensity noise (i.e., phase-induced intensity noise). An excellent match between experiment and simulation is shown for up to four simultaneous users. Based on this agreement between simulation and experiment, a prediction of potential system capacity is made.

The remainder of the paper is organized as follows. In Section II, the supermiposed FBG fabrication is presented. Section III presents the experimental setup and results. In Section IV, predictions of BER performance are made by analysis of the various noise sources. Finally, in Section V, the performance of FE-OCDMA is investigated with various modified system configurations, such as encoders without guard bands, Bragg gratings in transmission instead of reflection, and orthogonal codes that have fixed cross correlation, such as m-sequence, Hadamard, or modified quadratic congruence (MQC) codes.

II. Superimposed FBG Encoders

FE-OCDMA employs one-dimensional (1-D) codes applied in the frequency domain. No time delay is imposed between different frequencies of a given code. An elegant way of achieving FE encoders is by using superimposed FBGs in reflection [2], [13], [14]. In that configuration, each FBG is written at the same location in the fiber in order to avoid delays between the multiple frequency components that are reflected. Writing superimposed FBGs is challenging, as each spectral band of a code must have the same bandwidth and reflectivity, while simultaneously maximizing the reflectivity. Moreover, the encoder/decoder pair has to be as identical as possible to properly recover the signals.

The superimposed FBGs corresponding to the FE-OCDMA codes are written using a frequency-doubled continuous-wave (CW) argon ion laser and a Sagnac interferometric setup [15]. The fiber is a photosensitive specialty fiber with hydrogen loading. Strong gratings are required to limit the insertion losses of the encoders, but, at the same time, the photosensitivity of the fiber must not be saturated in order to ensure uniform reflectivity of all the spectral bands. The first gratings are written several decibels stronger than the last ones, as their corresponding modulation index is partially erased by the other gratings during the writing process. Each grating is 2 cm long and has a sinc main-lobe apodization.

For frequency encoding, an m-sequence code [12] is used, which in theory allows for the complete elimination of MAI when combined with balanced detection. The code length is 15, and its weight 8. The frequency bins are spaced 50 GHz apart

Manuscript received January 30, 2004; revised April 15, 2004. This work was supported in part by the Natural Sciences and Engineering Research Council of Canada (NSERC) under Grant CG029055 and PADCO FT076892. This material was present in part at the IEEE International Conference Communications (ICC 2004), Paris, France, June 20–24, 2004, and at Conference on Bragg Gratings, Poling & Photosensitivity in Glass Waveguides (BGPP), September 1–3, 2003, Monterey, CA.

S. Ayotte, J. Magné, L. A. Rusch, and S. LaRochelle are with the Centre d'Optique Photonique et Laser (COPL), Department of Electrical and Computer Engineering, Université Laval, Québec, QC G1K 7P4, Canada (e-mail: rusch@gel.ulaval.ca).

M. Rochette is with the Centre of Excellence for Ultrahigh-bandwidth Devices for Optical Systems (CUDOS), Photonics and Optical Physics Laboratory (POPLUS), School of Physics, University of Sydney, Sydney, NSW 2006 Australia.

Digital Object Identifier 10.1109/JLT.2004.839984

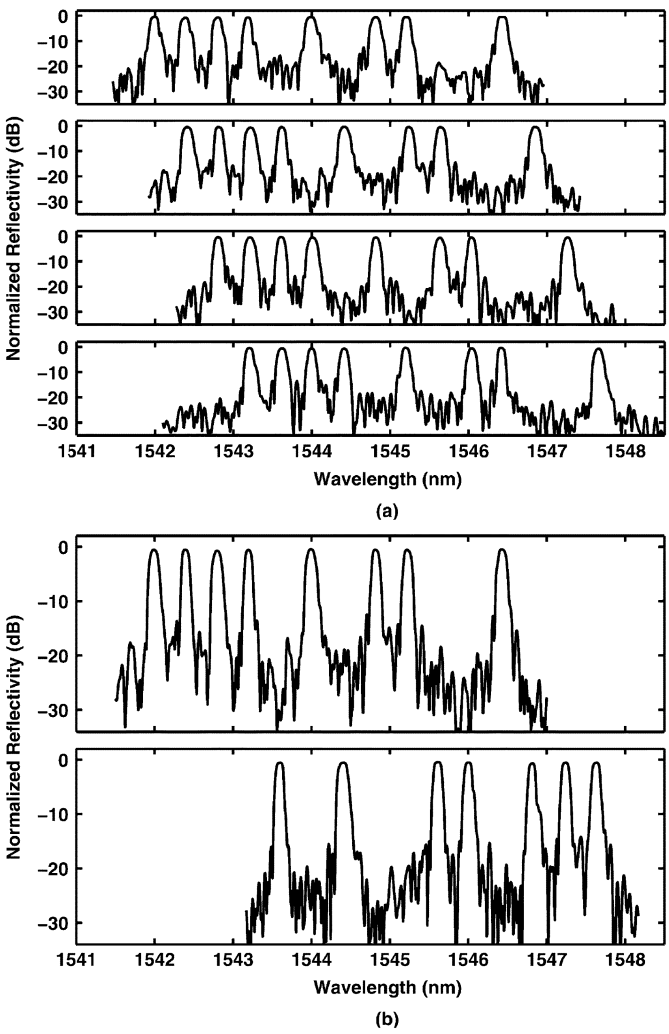

Fig. 1. (a) Spectral response of the four encoders, and (b) the decoder and complementary decoder.

and range from 1542.0 to 548.0 nm. In order to perform preliminary tests of the proposed system, only four users are experimentally implemented, although the proposed codes might accommodate up to 15 users. In the system, user 1 is chosen as the desired user, and users 2, 3, and 4 are interferers. The spectral response of the encoders is displayed in Fig. 1(a). Two additional superimposed FBGs, one corresponding to the code of user 1 and one corresponding to its complement, are fabricated for the decoding operation, and their spectral response is shown in Fig. 1(b). The corresponding logical equivalent of these codes is shown in the inset of Fig. 2. The reflectivity of the individual gratings is $85\pm5\%$, the bandwidth is 12.5 ± 1.5 GHz, and the accuracy of the peak frequency placement is ±2.2 GHz. Side-lobe suppression is 15 dB, while adjacent peak isolation is better than 20 dB.

The total index change in the superimposed FBGs is the sum of sinusoidal index modulations and can be expressed as

$$\Delta n(z) = \sum_{i=1}^{8} \left[\Delta n_i^{\mathrm{DC}}(z) + \Delta n_i^{\mathrm{AC}}(z) \cos\left(\frac{2\pi}{\Lambda_i} z + \varphi_i \right) \right] \quad (1)$$

where Δn_i^{DC} and Δn_i^{AC} are, respectively, the average and the oscillating parts of the refractive index change of the ith grating along the fiber axis z. The grating periods Λ_i are determined by the m-sequence code. In [13], simulation results on superimposed FBGs are presented assuming the individual gratings to be in phase ($\varphi_i = 0$ for all i). However, the parameter φ_i is difficult to control experimentally, and the grating phase is best modeled as a random variable. From (1), the total index change can be reduced to an equivalent grating with a refractive-index modulation having varying phase and amplitude

$$\Delta n(z) = \Delta n_{\Sigma}^{\mathrm{DC}}(z) + \Delta n_{\Sigma}^{\mathrm{AC}}(z) \cos\left(\frac{2\pi}{\Lambda_{\Sigma}} z + \theta_{\Sigma}(z) + \varphi_{\Sigma} \right) \quad (2)$$

where the symbol Σ refers to the sum-equivalent computed parameters [14]. From (2), a standard transfer matrix method may be used to numerically evaluate the spectral response. Since the equivalent grating is chirped and exhibits discrete phase shifts, a high number of segments is required to adequately sample the index modulation. The maximum peak-to-peak index change induced in the optical fiber is thus evaluated to be typically 2.8×10^{-3}.

III. Experimental Setup and Results

The experimental setup is shown in Fig. 2. At the transmitter, the erbium-doped broad-band fiber source has a power spectral density of -0.85 to -0.35 dBm/nm in the 1542.0–1548.0-nm spectral region. The source is modulated with a standard non-return-to-zero format using a $2^{23} - 1$ pseudorandom bit sequence. The optical signal then passes through a circulator and a 1×4 coupler before being reflected by four superimposed FBG encoders. This architecture emulates code-division multiple-access (CDMA) signals coming from four distinct users. The data streams are decorrelated using fiber delay lines of various lengths before the encoders. The multiplexed signals are then preamplified with an erbium-doped fiber amplifier (EDFA) that is chosen such that its combination with the broad-band source results in a flat spectrum at detection.

The power budget for this transmitter is given in Table I when only user 1 is active. The 26.7-dB loss incurred before the EDFA is due to the second pass through the polarization controller, 1×4 coupler, and circulator, plus the restrained spectral width of the encoder that only reflects a small part of the total source spectrum. Note that the power budget is meaningful before the EDFA because the signal before amplification must be high enough in order to have an amplified signal with a good extinction ratio. The EDFA provides adequate gain and, therefore, power budget after the EDFA is not detailed.

At the receiver, an attenuator is used to adjust the received signal power during BER measurements and to compensate the EDFA gain variations when changing the number of active users. The signals are copolarized by individually adjusting the polarization controllers placed before the encoders. This operation is verified by maximizing the power through a 10% tap coupler and a polarizer. Note that an alignment of the polarization among users leads to a worst-case situation for

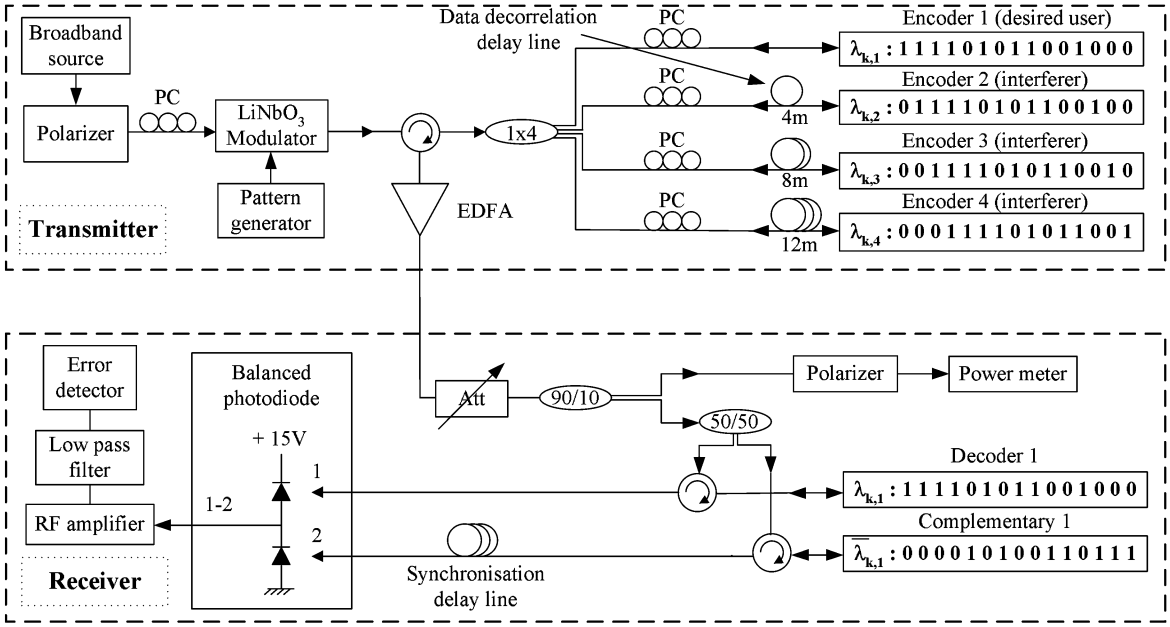

Fig. 2. Simultaneous users of the FE-OCDMA system with balanced detection. PC: Polarization controller; EDFA: erbium-doped fiber amplifier.

TABLE I
POWER BUDGET FOR USER 1

	Power [dBm]	Loss [dB]
Source	15.2	-
After Polarizer	11.4	3.8
After Polarization Controller	11.2	0.2
After Modulator (with data)	4.5	6.7
After Circulator	3.5	1.0
After Coupler 1x4	-3.5	7.0
After Polarization Controller	-4.1	0.6
Before EDFA	-30.8	26.7

BER performance but is used here to facilitate comparison between experimental and theoretical results. At the receiver side, the CDMA-coded signal is split by a 3-dB coupler, whose first output is connected to a decoder identical to encoder 1, whereas the second output is connected to a decoder that is the logical complement to encoder 1. A synchronization fiber delay line is placed after the complementary decoder in order to synchronize the signals in the two photodetector inputs. The 830-MHz balanced photodetector radio frequency (RF) output provides an electrical signal proportional to the power difference of the two optical inputs. The RF signal is amplified and low-pass-filtered to remove the out-of-band high-frequency noise. The bandpass of the filter is $B_e \approx 0.75 \times R_T$, where R_T is the transmission rate, and the shape of the transfer function is Bessel–Thomson of degree four.

Fig. 3 presents BER versus desired user power for this system with one, two, three, and four simultaneous users. The figure contains experimental results from the setup described in this section and simulation results following the methodology of Section IV. Note that the desired user power in the abscissa is the mean optical power difference between decoder 1 and complementary 1. The curves in Fig. 3(a) are for a transmission rate of 155 Mb/s, and those of Fig. 3(b) are for a rate of 622 Mb/s. In both graphs, no BER floor is noticeable for a single user system out to a BER of 10^{-12}. At 155 Mb/s, we see a BER floor for three users, and at 622 Mb/s, the floor is apparent with only two users. At low power, the system is dominated by detection noises, whereas at high power, it is dominated by intensity noise that is signal dependent. Therefore, when intensity noise is important, increasing the received power cannot improve the BER and floors appear. Recall, these experimental results are not optimized to show maximum system capacity (see Section V) but rather to validate theoretical and simulation results.

Fig. 4 allows a better understanding of the intensity noise dependences when the number of active users increases; it shows the eye diagrams for one and four simultaneous users at a transmission rate of 155 Mb/s and high power. With one active user, the intensity noise on the "1" level is dominant over the noise on the "0." However, the eye is still opened, and error-free transmission is possible. With four users, important intensity noise emerges on both "0" and "1," the eye is narrowed, and errors appear. The balanced detection cancels the MAI, but the intensity noises on both photodiodes are additive. For m-sequences, each pair of users has half their frequencies in common. When increasing the number of interferers, the energy incident on the photodiodes causes significant intensity noise.

IV. BER ANALYSIS

Modeling of the noises present in an FE-OCDMA system is necessary to understand the main system limitations and to allow the design of optimized systems. In order to tighten the correspondence between results and theory, all the noises that might influence the system performance are considered in this section. In the following subsections, the mathematical model of each noise source and the experiments used to parameterize these models are presented.

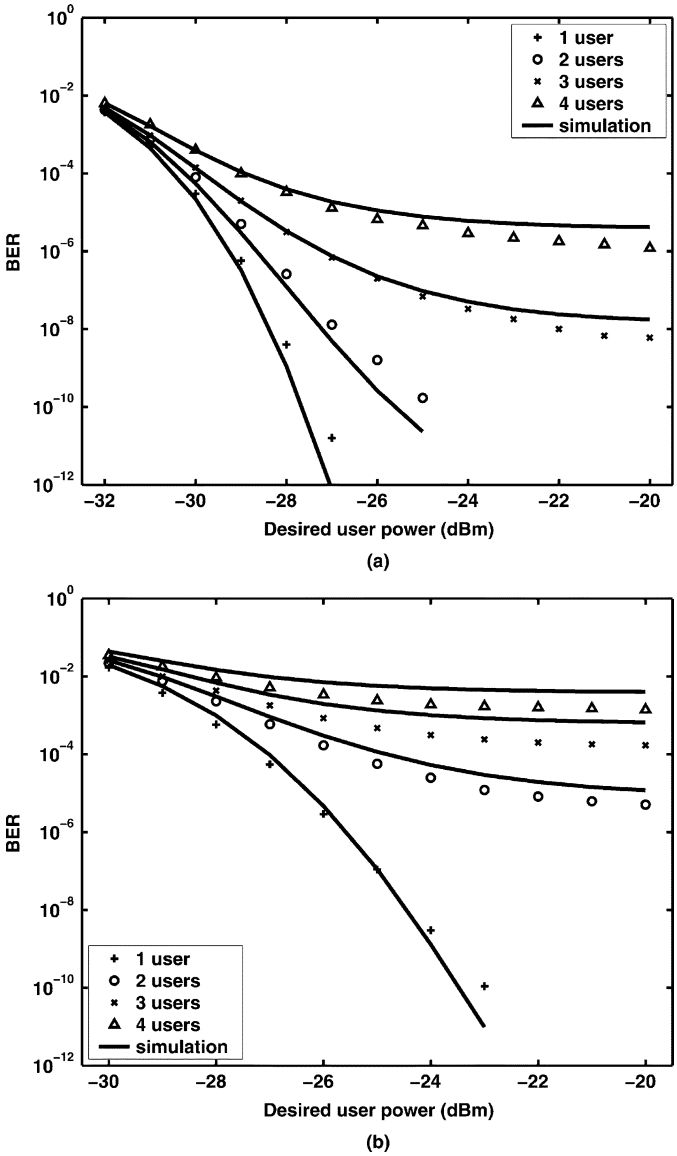

Fig. 3. BER versus desired user power for transmission rates of (a) 155 Mb/s and (b) 622 Mb/s.

A. Intensity Noise

The most important noise for the system at high optical power is the intensity noise associated with the use of incoherent broad-band sources. This noise is power dependent so that increasing the signal power does not improve the signal-to-intensity-noise ratio (SNR). The intensity noise can be modeled for a given SNR (γ) by a gamma distribution [16]. Therefore, the conditional probability density function (pdf) of the integrated optical power W, when conditioned on the average integrated optical power $\bar{W}$, for $W \geq 0$ is given by

$$f(W|\bar{W}) = (\gamma/\bar{W})^{\gamma} \frac{W^{\gamma-1} \exp\left(-W\gamma/\bar{W}\right)}{\Gamma(\gamma)} \tag{3}$$

where Γ is the usual gamma function and where the integrated optical power W corresponds to the time integral of the instantaneous optical power I over the time constant of the electrical filter T

$$W(t) = \int_{t-T}^{t} I(\varepsilon) d\varepsilon. \tag{4}$$

Note that in [16], W has units of [W/m^2], whereas in this analysis, the surface area is constant; thus, W has units of [W] and all measurements are made in [W]. Furthermore, parameters presented in the next subsections are consistent with W in [W] for (8)–(10).

We next derive an expression for γ in the intensity noise pdf. For electrical and optical filters of arbitrary spectral shapes, the power spectral density (PSD) of both the signal and intensity noise are given in [17]. In this case, the PSD of the noise is the autocorrelation of the optical spectrum, and the signal power is the square of the integrated optical spectrum. The resulting SNR is thus given by

$$\gamma = \frac{m \cdot H(0) \left(\int_{-\infty}^{\infty} S(\upsilon)\, d\upsilon \right)^2}{\int_{-\infty}^{\infty} \left(\int_{-\infty}^{\infty} S(\upsilon) S(\upsilon + f)\, d\upsilon \right) H(f)^2 df} \tag{5}$$

where υ and f are the optical and baseband frequencies, respectively, $S(\upsilon)$ is the optical spectrum, $H(f)$ is the electrical filter transfer function, and where $m = 1$ for a polarized signal and $m = 2$ for an unpolarized signal. This expression for γ is equivalent to that in [16] for a polarized signal. Moreover, it allows the use of any arbitrary electrical filter profile. For optical and electrical filters having a rectangular shape, it can be shown that the SNR is $\gamma = mB_o^2/(2B_o - B_e)B_e$ [18], where B_o and B_e are the optical and electrical bandwidth, respectively. For $B_o \gg B_e$, the SNR is approximated by $\gamma \approx mB_o/2B_e$.

B. Other Noise Sources

The noise from the modulating system (pattern generator and modulator) was found to have a nonnegligible impact on the system. Therefore, this noise is characterized using a digital communication analyzer (DCA); it is modeled as having a Gaussian distribution. That is, the average integrated optical power $\bar{W}$ is pattern dependent and varies from bit to bit with a normal distribution whose mean and variance is measured experimentally. As this modulation noise appears before detection of the FE-OCDMA signal, the intensity noise at detection is dependent on it, and this dependence is treated in the next subsection.

The photodetector thermal noise, the RF amplifier noise, and the error detector intrinsic noise are also considered. All are assumed to be Gaussian and independent of one another. The photodetector thermal noise is measured directly with a DCA. The RF amplifier noise and gain are also characterized with the DCA for different input levels. The error detector intrinsic noise is measured by connecting the pattern generator to the error detector without having to modulate any optical signal. A pattern composed exclusively of "1"s is sent, and the errors are detected at different thresholds. This measurement provides the cumulative distribution function of the voltage noise around the threshold.

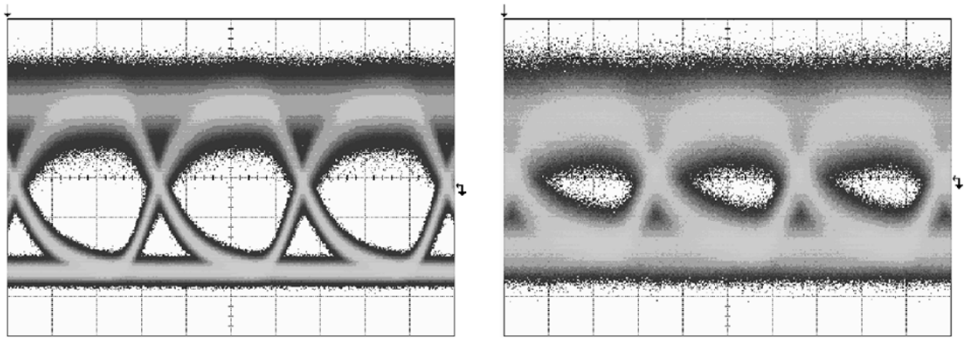

Fig. 4. Eye diagrams for (a) one and (b) four users ($R_t = 155$ Mb/s).

C. Noise Dependencies

In order to predict the BER, the resultant pdf, including all the noise sources, must be calculated. As discussed in the previous subsections, intensity noise is the dominant noise source in systems using incoherent sources, and its contribution strongly depends upon the shape of the optical spectrum at the photodiodes. For the FE-OCDMA system studied here, the shape of the optical spectrum at both inputs of the balanced photodetector depends on the number of active users and on the bits sent by them. If K users are active, there are 2^K possible spectrum shapes at the input of each photodiode. By measuring the optical spectrum incident on each of the two photodiodes for each user taken one at a time, the corresponding optical spectrum for any given combination of bits can be deduced.

The column vectors $\underline{F_1}(\upsilon) = [F_1^1(\upsilon)\ F_1^2(\upsilon)\ \cdots\ F_1^K(\upsilon)]^T$ and $\underline{F_2}(\upsilon) = [F_2^1(\upsilon)\ F_2^2(\upsilon)\ \cdots\ F_2^K(\upsilon)]^T$ represent the spectrum of each user measured individually after the decoder (subscript 1) and the complementary decoder (subscript 2), respectively. We use $\underline{\hat{F}_1}(\upsilon)$ and $\underline{\hat{F}_2}(\upsilon)$ to represent these spectra once normalized by the optical power of the desired user.

Next, the pdf for the decoder branch is developed; the procedure is identical for the complementary decoder branch. Let $\underline{d}$ be the binary column vector of data bits, where d_i is the bit of the ith user. The optical spectrum after the decoder is

$$S_{1,\underline{d}}(\upsilon) = \underline{d}^T \cdot \underline{\hat{F}_1}(\upsilon). \tag{6}$$

Note that since the extinction ratio is not ideal, d_i takes the value 1 for a logical "1" and $1/E_{\rm dec}$ for a logical "0", where $E_{\rm dec}$ is the extinction ratio after the decoder and its experimental value is given in Table II.

We calculate $\gamma_{1,\underline{d}}$ (again, subscript 1 refers to the decoder branch) by substituting $S_{1,\underline{d}}(\upsilon)$ in (5) for a given $\underline{d}$. The vector of data bits also influences the average integrated optical power; hence, we write $\bar{W}_{\underline{d}}$. The average integrated optical power has a Gaussian distribution; $\bar{W}_{\underline{d}} \sim \eta(\mu_{\underline{d}}, \sigma_{\underline{d}})$, where $\mu_{\underline{d}}$ is calculated from $\mu_{\underline{d}} = \int_{-\infty}^{\infty} S_{1,\underline{d}}(\upsilon)d\upsilon$, μ/σ is measured experimentally, as given in Table II, and $\mu_{\underline{d}}/\sigma_{\underline{d}} = \mu/\sigma, \forall \underline{d}$.

Let $W_{1,\underline{d}}$ be the random variable that represents the integrated optical power at the decoder when bit pattern $\underline{d}$ is sent. The conditional pdf for $W_{1,\underline{d}}$ is given in (3) as parameterized with $\gamma_{1,\underline{d}}$ and the average integrated optical power $\bar{W}_{\underline{d}}$. The unconditioned pdf of $W_{1,\underline{d}}$ can be computed by integrating numerically the conditional pdf over the pdf of $\bar{W}_{\underline{d}}$,

$$f(W_{1,\underline{d}}) = \int_{-\infty}^{\infty} f(W_{1,\underline{d}}|\bar{W}_{\underline{d}}) f(\bar{W}_{\underline{d}}) d\bar{W}_{\underline{d}}. \tag{7}$$

The pdf at the complementary decoder is found from $\underline{\hat{F}_2}(\upsilon)$ following the same steps, and the pdfs are computed for the output of each of the two photodiodes. The decision statistic at the receiver is

$$z_{\underline{d}} = W_{1,\underline{d}} - W_{2,\underline{d}} + n \tag{8}$$

where n represents the noise coming from the photodetector, RF amplifier, and error detector, whereas the intensity and modulation noises are included into $W_{1,\underline{d}}$ and $W_{2,\underline{d}}$. The noise n is modeled as independent additive white Gaussian noise (AWGN) with zero mean and variance σ_n^2 that is measured experimentally

$$\sigma_n^2 = \frac{1}{(R_{\rm PD})^2}\left(\sigma_{\rm PD}^2 + \frac{\sigma_{\rm RF}^2}{G_{\rm RF}} + \frac{\sigma_{\rm ED}^2}{G_{\rm RF}}\right) \tag{9}$$

where $\sigma_{\rm PD}, \sigma_{\rm RF}$, and $\sigma_{\rm ED}$ are the noises from the balanced photodiode, the RF amplifier, and the error detector, respectively. $R_{\rm PD}$ corresponds to the responsivity times the gain of the photodiode, whereas $G_{\rm RF}$ is the gain of the RF amplifier. $R_{\rm PD}$ and $G_{\rm RF}$ allow us to express σ_n in optical [W], the same units as W. Detection noises are taken into account because they become nonnegligible at low power levels. Their contribution is evaluated, and the measured values for the parameters in (9) are presented in Tables II–IV.

TABLE II
MEASURED NOISE PARAMETERS

		R_T=155 Mb/s	R_T=622 Mb/s
Modulation noise	μ/σ	35.5 (15.5 dB)	44.4 (16.5 dB)
Balanced photodiode	R_{PD}	690 V / W	710 V / W
	σ_{PD}	142 μV	297 μV
Error detector	σ_{ED}	550 μV	550 μV
Optical extinction ratio			
After modulator	-	39.0 (15.9 dB)	26.3 (14.2 dB)
After decoder	E_{dec}	18.3 (12.6 dB)	12.4 (10.9 dB)

TABLE III
RF AMPLIFIER CHARACTERIZATION ($R_T = 155$ Mb/s)

$V_1 - V_0$ ΔV_{in} [mV]	Gain $10\times log(G_{RF})$ [dB]	Noise on "0" σ_{RF} [mV]	Noise on "1" σ_{RF} [mV]
0.76	31.7	0.73	0.77
1.07	31.9	0.77	0.83
2.40	31.8	0.90	1.15
4.79	31.8	1.16	1.87
7.18	31.6	1.16	2.46
14.30	31.6	1.71	5.13

TABLE IV
RF AMPLIFIER CHARACTERIZATION ($R_T = 622$ Mb/s)

$V_1 - V_0$ ΔV_{in} [mV]	Gain $10\times log(G_{RF})$ [dB]	Noise on "0" σ_{RF} [mV]	Noise on "1" σ_{RF} [mV]
0.72	31.4	0.96	1.19
1.44	31.2	1.18	1.67
2.28	31.5	1.61	2.52
4.55	31.3	2.70	4.64
7.20	31.1	4.79	7.14
14.37	31.0	7.97	14.24

In order to calculate the pdf of the decision statistic, the integrated optical power at the output of the decoder $W_{1,\underline{d}}$ is considered to be independent of the output from the complementary decoder $W_{2,\underline{d}}$; this assumption is reasonable as the power comes from different spectral regions. Thus, the pdf of the decision statistic is the convolution of the pdfs

$$f(z_{\underline{d}}) = f(W_{1,\underline{d}}) * f(-W_{2,\underline{d}}) * f(n). \tag{10}$$

An average over the distribution of equiprobable bit patterns $\underline{d}$ finally leads to

$$f(z \,|\, d_1 = 0) = \frac{1}{2^{K-1}} \sum_{\underline{d}(d_1=0)} f(z_{\underline{d}}) \tag{11a}$$

$$f(z \,|\, d_1 = 1) = \frac{1}{2^{K-1}} \sum_{\underline{d}(d_1=1)} f(z_{\underline{d}}). \tag{11b}$$

The BER is calculated by integrating the tails of these final pdfs, as follows:

$$\text{BER} = \frac{1}{2} \int_{\eta}^{\infty} f(z \,|\, d_1 = 0) dz + \frac{1}{2} \int_{-\infty}^{\eta} f(z \,|\, d_1 = 1) dz \tag{12}$$

where η is the threshold; numerical methods are used to find the optimal threshold. This BER is for a particular number of active users and for a particular desired user power.

In the experiment, the BER is measured for up to four simultaneous users, and the noise analysis presented in this section is used to generate the simulation curves on Fig. 3. An excellent match is found between simulation and experiment. The slight differences at high power might come from the calculation of the intensity noise that assumes a Bessel–Thomson filter instead of the exact transfer function of the whole electrical system. In addition, the polarizations of the four users have been coaligned but with a limited precision, possibly causing lower BER than predicted.

V. PREDICTION OF FE-OCDMA CAPACITY

In the previous section, we show that the intensity noise from incoherent broad-band sources causes a serious limitation to the system performance. In order to better define the exact limitation and to predict the performances of an optimized system, we present results from a computer simulator that considers only the intensity noise. For ease of interpreting results, we consider optical slices and electrical filters of ideal rectangular shapes. FBGs, or any frequency-selective components, are simulated either in reflection or in transmission, and the optical signal is taken as unpolarized. We simulate both unipolar as well as bipolar systems. For both modes, when a logical "1" is transmitted, light is sent to the encoder. For the unipolar case, when a logical "0" is transmitted, nothing is sent, while for the bipolar case, a logical "0" is represented by light sent to the complementary encoder. The experimental validation of our simulation allows us to predict with confidence the performance attainable when optimizing system parameters that were not available for this experiment. Several lessons are clear, as described hereafter.

The analysis of FE-OCDMA capacity given in [9] is confirmed by our experiments and simulations. As proposed in [9], a code that partitions all the available optical bandwidth yields the best system performance. Due to our concern for reducing MAI and also due to the complexity of writing superimposed FBGs, significant guard frequencies were employed in our experiment between frequency bins in the code so that only 25% of the available optical bandwidth was used. In addition, the Hadamard codes proposed by [8] and [9] and m-sequence codes used in our experiments do not yield optimal performance.

As proposed in [10] and [11], the MQC codes offer significant improvement over Hadamard codes by reducing intensity noise and maintaining code orthogonality for a receiver using balanced detection. While [10] and [11] predictions of BER are optimistic, based on our experimental and simulation results, they still offer considerable performance improvement, on the order of twice the capacity of Hadamard codes. Details are provided in the following discussion.

As proposed in [7], FE-OCDMA can be accomplished using FBGs in transmission, simplifying the technical demands on FBG fabrication and enabling the use of MQC codes. The capacity predictions in [7] are overly optimistic, as the FBGs used are too narrow to be used in transmission; a large uncoded energy is transmitted, increasing intensity noise. That energy is incident both on the decoder and the complementary decoder and does not contribute to the signal but only to the noise. In addition, the analysis used to predict capacity is that of [9], while the encoders used in fact included significant guard frequencies that would reduce system performance.

Taking into account these lessons, in Fig. 5, we present simulation results for systems with bit rates of 155 Mb/s, 415 Mb/s, 622 Mb/s, and 1.25 Gb/s. We assume the use of encoders/decoders with square frequency bins, MQC codes, and a code that partitions the entire available optical bandwidth (10 and 30 nm are simulated). The MQC codes have a weight of $p + 1$ and a length of $p(p + 1)$. Therefore, an available optical bandwidth of B_o would be partitioned into logical frequency bins of width $B_o/p(p+1)$. However, a code consists of $p+1$ peaks of one bin width and $p + 2$ gaps of various multiples of a bin width. When

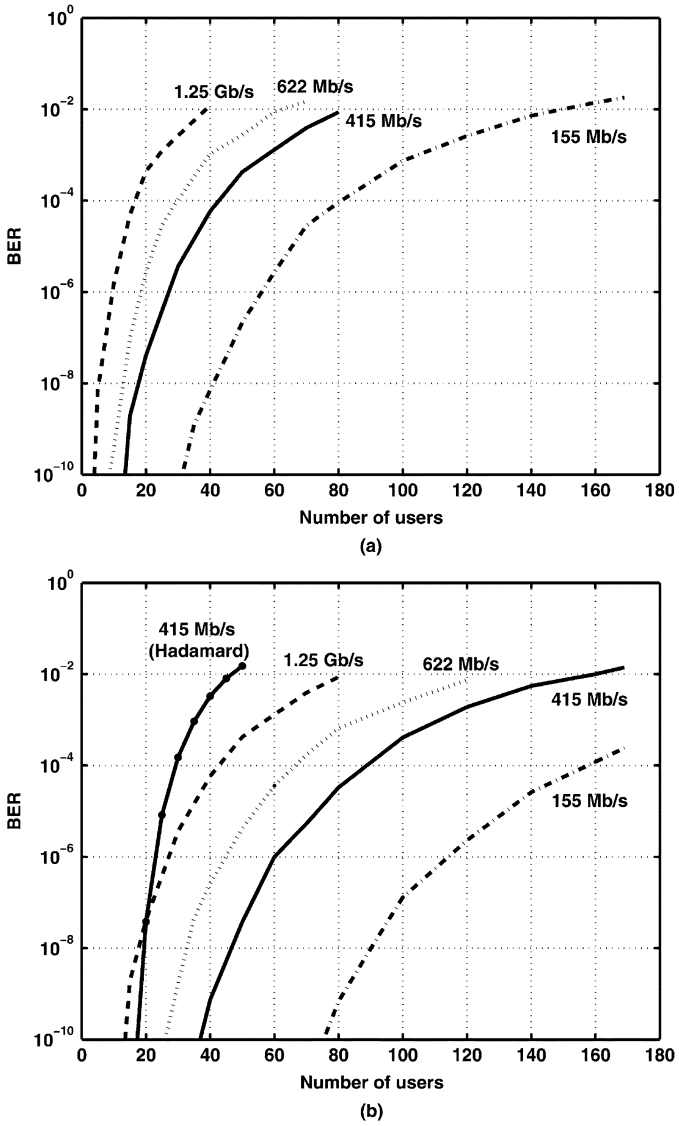

Fig. 5. BER versus number of users for MQC codes ($p = 13$), various transmission rates, and optical bandwidths of (a) 10 nm and (b) 30 nm.

writing an encoder as an FBG in transmission, we would have $p+2$ peaks of various multiples of a bin width and $p+1$ gaps of one bin width. We select $p = 13$ because of its reasonable fabrication complexity and good system capacity. In Fig. 5(a), we present the BER versus the number of system users when the available bandwidth is 10 nm; the long dashed line is for transmission rate of 1.25 Gb/s, the short dashed line 622 Mb/s, the solid curve 415 Mb/s, and the dashed–dotted line 155 Mb/s. The same data are presented in Fig. 5(b) for $2B_o = 30$ nm plus a solid dotted curve that represents Hadamard codes at 415 Mb/s.

The MQC codes proposed by [10] and [11] have lower fixed cross correlation than Hadamard codes. Therefore, they should be less subject to intensity noise. These codes must be used in a unipolar system and are orthogonal when combined with balanced detection. Theoretical predictions have been made by [10] based on the model developed by [9]. We refine their BER calculations as, in a unipolar system [10], [11] as opposed to a bipolar one [9], there are many different pdfs possible after the balanced detection depending on the data vector $\underline{d}$ sent, and each of these must be considered in the BER calculation.

In [11], an MQC code ($p = 13$) with an optical bandwidth of 30 nm in a unipolar unpolarized system at a transmission rate of 622 Mb/s ($B_e = 311$ MHz) is predicted to support approximately 55 users with a BER of $\sim 10^{-9}$. We introduce these parameters in the simulator with $R_T = 415$ Mb/s and $B_e = 311$ MHz (in the simulator, the electrical filter is $B_e \sim 0.75 \times R_T$, whereas in [9]–[11], it is taken to be $B_e \sim 0.50 \times R_T$). A maximum of 42 users [Fig. 5(b)] could be accommodated, while a bipolar system with Hadamard codes could only support up to 18 users [Fig. 5(b)] at such a BER. Even if the predictions of [10] and [11] are too optimistic, the proposed codes can considerably improve the performance of an FE-OCDMA system, as shown by the $R_T = 415$ Mb/s curves.

When simulating the system described in [7], assuming unpolarized light, which should give the best results, it is found that such a system could accommodate less than half of the users predicted by [7]. Nevertheless, the proposition in [7] to use the FBGs in transmission has great merit as it allows the writing of gratings in cascade as opposed to superimposing them in the fiber. In transmission, there is no delay imposed by the FBGs. This allows more flexibility in the codes, as the number of FBGs placed in series and their optical bandwidth are unlimited. Furthermore, the use of chirped gratings also provides an additional degree of freedom in tailoring the optical bandwidth of the encoders. In conclusion, an optimized FE-OCDMA system with incoherent sources and balanced detection would use low fixed cross-correlation codes, and the whole optical bandwidth would be used in order to reduce intensity noise.

VI. Conclusion

A novel and simple coding approach using superimposed FBGs to achieve FE-OCDMA is demonstrated experimentally as well as theoretically. A good MAI rejection is obtained using balanced photodetection. This system is limited by the intensity noise inherent to the incoherent FE-OCDMA approach. A simulator is developed and its accuracy is validated by a comparison with both experimental results and an analytical prediction [9]. It is shown that codes using low fixed cross-correlation combined with FBGs in transmission using the whole optical bandwidth could improve the performance of an FE-OCDMA system. These optimized parameters can significantly reduce the effect of intensity noise but cannot eliminate it completely. Future work should focus on decreasing the intensity noise effect by using components such as coherent sources and nonlinear detection.

Acknowledgment

The authors would like to thank Dr. D. Wei for many helpful discussions.

References

[1] D. M. Meghavoryan and H. V. Baghdasaryan, "Code-division multiple access: Novel multiplexing strategy in optical fiber networks," in *Proc. Int. Conf. Transparent Optical Networks (ICTON)*, 2001, pp. 299–303.

[2] J. Magné, D.-P. Wei, S. Ayotte, L. A. Rusch, and S. LaRochelle, "Experimental demonstration of frequency-encoded optical CDMA using superimposed fiber Bragg gratings," in *Proc. Conf. Bragg Gratings, Poling & Photosensitivity in Glass Waveguides (BGPP)*, 2003, pp. 294–296.

[3] J. F. Huang and C. C. Yang, "Reductions of multiple-access interference in fiber-grating-based optical CDMA network," *IEEE Trans. Commun.*, vol. 50, no. 10, pp. 1680–1687, Oct. 2002.
[4] T. Pfeiffer, B. Deppisch, M. Kaiser, and R. Heidemannm, "High speed optical network for asynchronous multiuser access applying periodic spectral coding of broadband sources," *Electron. Lett.*, vol. 33, pp. 2141–2142, Dec. 1997.
[5] C. F. Lam, D. T. K. Tong, M. C. Wu, and E. Yablonovitch, "Experimental demonstration of bipolar optical CDMA system using a balanced transmitter and complementary spectral encoding," *IEEE Photon. Technol. Lett.*, vol. 10, pp. 1504–1506, Oct. 1998.
[6] T. Dennis and J. F. Young, "Measurement of BER performance for bipolar encoding of an SFS," *J. Lightw. Technol.*, vol. 17, no. 9, pp. 1542–1546, Sep. 1999.
[7] G. A. Magel, G. D. Landry, R. J. Baca, D. A. Harper, and C. A. Spillers, "Transmission of eight channels × 622 Mb/s and 15 channels × 155 Mb/s using spectral encoded optical CDMA," *Electron. Lett.*, vol. 37, pp. 1307–1308, Oct. 2001.
[8] M. Kavehrad and D. Zaccarin, "Optical code-division-multiplexed systems based on spectral encoding of noncoherent sources," *J. Lightw. Technol.*, vol. 13, no. 3, pp. 534–545, Mar. 1995.
[9] E. D. J. Smith, R. J. Blaikie, and D. P. Taylor, "Performance enhancement of spectral-amplitude-coding optical CDMA using pulse-position modulation," *IEEE Trans. Commun.*, vol. 46, no. 9, pp. 1176–1185, Sep. 1998.
[10] Z. Wei, H. M. H. Shalaby, and H. G. Shiraz, "Modified quadratic congruence codes for fiber Bragg-grating-based spectral-amplitude-coding optical CDMA systems," *J. Lightw. Technol.*, vol. 19, no. 9, pp. 1274–1281, Sep. 2001.
[11] Z. Wei and H. G. Shiraz, "Codes for spectral-amplitude-coding optical CDMA systems," *J. Lightw. Technol.*, vol. 20, no. 8, pp. 1284–1291, Aug. 2002.
[12] R. L. Peterson, R. E. Ziemer, and D. E. Borth, *Introduction to Spread Spectrum Communications*. Englewood Cliffs, NJ: Prentice-Hall, 1995.
[13] D. M. Meghavoryan and A. V. Daryan, "Superimposed fiber Bragg grating simulation by the method of single expression for optical CDMA systems," *IEEE Photon. Technol. Lett.*, vol. 15, no. 11, pp. 1546–1548, Nov. 2003.
[14] M. Popov, F. Carlsson, P.-Y. Fonjallaz, J. Skaar, G. Concas, and S. Helmfrid, "Design and fabrication of superimposed fiber Bragg gratings: Models, methods, and limitations," in *Proc. Photosensitivity Optical Waveguides and Glasses (POWAG) 2002*, pp. 34–36.
[15] S. LaRochelle, P. Y. Cortes, H. Fathallah, L. A. Rusch, and H. B. Jaafar, "Writing and applications of fiber Bragg grating arrays," in *Proc. SPIE*, vol. 4087, Jun. 2000, pp. 140–149.
[16] J. W. Goodman, *Statistical Optics*. New York: Wiley, 2000.
[17] G.-H. Duan and E. Georgiev, "Non-white photodetection noise at the output of an optical amplifier: Theory and experiment," *IEEE J. Quantum Electron.*, vol. 37, no. 8, pp. 1008–1014, Aug. 2001.
[18] P. C. Becker, N. A. Olsson, and J. R. Simpson, *Erbium-Doped Fiber Amplifiers Fundamentals and Technology*. San Diego, CA: Academic, 1999.
[19] S. Ayotte, M. Rochette, J. Magné, L. A. Rusch, and S. LaRochelle, "Experimental demonstration and simulation results of frequency encoded optical CDMA," in *IEEE Int. Conf. Communications (ICC 2004)*, vol. 3, Jun. 20–24, 2004, pp. 1704–1708.

Simon Ayotte (S'04) was born in Québec, QC, Canada, in 1979. He received the B.S. degree in engineering physics from Université Laval, Québec, QC, Canada, in 2002. He is currently working toward the Ph.D. degree in optical telecommunications with a dissertation on optical-code-division multiple access (O-CDMA) at the Centre d'Optique, Photonique et Lasers, Department of Electrical and Computer Engineering, Université Laval.

His research interests include fiber-optic communication systems and O-CDMA.

Mr. Ayotte is a Student Member of the Optical Society of America (OSA).

Martin Rochette received the B.S. degree in engineering physics and the M.Sc. and Ph.D. degrees in electrical and computer engineering from Université Laval, Québec, QC, Canada, in 1995, 1997, and 2001, respectively.

He conducted research on functional aspects of Bragg gratings such as gain flattening of erbium-doped fiber amplifiers (EDFAs) and polarization-mode-dispersion (PMD) compensation of chirped Bragg gratings. He also conducted research on optical communication systems test beds to measure/compensate the impact of long-distance transmission of optical pulses in the presence of gain nonuniformity arising from EDFAs, chromatic dispersion, and stochastic and deterministic PMD. Since 2001, his research has focused on the modeling of bit-error ratio in code-division multiple-access (CDMA) systems and wavelength-division-multiplexed systems.

Julien Magné was born on April 6, 1977. He received the B.S. degree in engineering optics from the Ecole Nationale Supérieure de Science Appliquée et Technologie (ENSSAT), Lannion, France. He is currently working toward the Ph.D. degree in electrical engineering, with a dissertation on erbium-doped fiber lasers, at the Université Laval, Québec, QC, Canada.

His research interests include fiber lasers, mode-locked fiber lasers, fiber Bragg gratings, and laser physics.

Leslie A. Rusch (S'91–M'94–SM'00) received the B.S.E.E. degree (with honors) from the California Institute of Technology, Pasadena, in 1980 and the M.A. and Ph.D. degrees in electrical engineering from Princeton University, Princeton, NJ, in 1992 and 1994, respectively.

She formerly spent two years (2001–2002) at Intel Corporation as the manager of a group researching new wireless technologies. She is currently a Professor in the Department of Electrical and Computer Engineering at Université Laval, QC, Canada, performing research on wireless and optical communications. Her research interests include optical-code-division multiple access using noncoherent sources for metropolitan-area networks; semiconductor and erbium-doped optical amplifiers and their dynamics; and in wireless communications, high-performance reduced-complexity receivers for ultrawide-band systems employing code-division multiple access.

Dr. Rusch is a Member of the Optical Society of America (OSA).

Sophie LaRochelle (M'00) received the B.S. degree in engineering physics from Université Laval, Québec, QC, Canada, in 1987 and the Ph.D. degree in optics from the University of Arizona, Tucson, in 1992.

She was a Research Scientist at the Defense Research Establishment Valcartier, Valcartier, QC, Canada, from 1992 to 1996, where she worked on electrooptical systems. She is currently a Professor with the Department of Electrical and Computer Engineering, Université Laval, where she holds the Canada Research Chair in Optical Fiber Communications and Components. Her current research activities are focused on active and passive fiber-optic components for optical communication systems, including fiber Bragg gratings, optical amplifiers, and multiwavelength and pulsed fiber lasers. His other research interests include optical-code-division multiple-access systems and nonlinear pulse propagation.

Dr. LaRochelle is a Member of the Optical Society of America (OSA).